Intermetallics

Volume 30, November 2012   **including metallic glasses**   ISSN 0966–9795

ELSEVIER   http://www.elsevier.com/locate/intermet

Corrosion resistance and biocompatibility of Ni-free Zr-based bulk metallic glass for biomedical applications

Her-Hsiung Huang [a,b,c,*], Ying-Sui Sun [d], Chia-Ping Wu [d], Chia-Fei Liu [d], Peter K. Liaw [e], Wu Kai [f]

[a] Department of Dentistry, National Yang-Ming University, Taipei, Taiwan
[b] Department of Dentistry, Taipei City Hospital, Taipei, Taiwan
[c] Department of Stomatology, Taipei Veterans General Hospital, Taipei, Taiwan
[d] Institute of Oral Biology, National Yang-Ming University, Taipei, Taiwan
[e] Department of Materials Science and Engineering, The University of Tennessee, Knoxville, TN, USA
[f] Institute of Materials Engineering, National Taiwan Ocean University, Keelung, Taiwan

ARTICLE INFO

ABSTRACT

Aim: Currently, the potential applications of Ni-free bulk metallic glasses (BMGs) in biomedical fields that have been reported in the literature are still limited. In this study, the corrosion resistance and biocompatibility of Ni-free, Zr-based $Zr_{50}Cu_{43}Al_7$ BMGs in biological environments were investigated.
Methods: The corrosion resistance was evaluated using potentiodynamic polarization curve measurements in simulated biological environments. The cytotoxicity was evaluated according to specification 10993-5 from the International Organization for Standardization (ISO). The protein (albumin) adsorption was evaluated using the bicinchoninic acid (BCA) assay. The adhesion and *in situ* migration of human bone marrow mesenchymal stem cells (hMSCs) were also evaluated.
Results: The main component on the outermost surface of $Zr_{50}Cu_{43}Al_7$ BMG was ZrO_2, with trace amounts of Cu and Al oxides. The corrosion rates of $Zr_{50}Cu_{43}Al_7$ in artificial saliva and in simulated body fluid were comparable with those of biomedical Ti metal in the same environments; however, pitting corrosion was observed on $Zr_{50}Cu_{43}Al_7$ in both environments. The cytotoxicity analysis results showed that $Zr_{50}Cu_{43}Al_7$ was nontoxic. Compared with Ti metal, $Zr_{50}Cu_{43}Al_7$ had a higher level of protein adsorption and better cell adhesion and cell migration.
Conclusion: $Zr_{50}Cu_{43}Al_7$ BMG has the potential to be used in biomedical applications because of its corrosion resistance and cellular responses. However, further improvements to the pitting corrosion resistance of $Zr_{50}Cu_{43}Al_7$ in biological environments should be made before proceeding to *in vivo* animal studies.

1. Introduction

Zr-based bulk metallic glasses (BMGs) have the potential to be used for biomedical applications and have attracted much interest in recent years. However, the Zr-based BMGs investigated in previous studies usually contain elemental Ni [1–5], which is possibly allergenic and carcinogenic to humans [6,7]. Recently, the biocompatibility of Ni-free, Zr-based BMGs has been investigated using mouse fibroblast cells [8–10]. However, biocompatibility assays using human cells and Ni-free, Zr-based BMGs would more closely resemble clinical conditions.

Furthermore, the elastic moduli of widely used biomedical Ti and its alloys are usually above 100 GPa, which is much higher than that of natural bone [11]. The difference in the elastic modulus between bone and metals may lead to the stress-shielding effect, which can cause bone resorption and problems for long-term use [12,13]. Thus, the development of biomaterials with elastic moduli closer to that of natural bone is an important issue in advanced orthopedic metals.

Recently, we successfully prepared a new Ni-free, Zr-based BMG with a composition of $Zr_{50}Cu_{43}Al_7$ and a lower elastic modulus of approximately 85 GPa. In this study, the corrosion resistance of $Zr_{50}Cu_{43}Al_7$ was evaluated in artificial saliva (SA) and in simulated body fluid (SBF). Cellular responses to $Zr_{50}Cu_{43}Al_7$ BMG, including adhesion and migration, were evaluated using human bone marrow mesenchymal stem cells (hMSCs).

* Corresponding author. Department of Dentistry, National Yang-Ming University, No. 155, Sec. 2, Li-Nong Street, Taipei 112, Taiwan. Tel.: +886 2 2826 7068; fax: +886 2 2826 4053.
E-mail address: hhhuang@ym.edu.tw (H.-H. Huang).

2. Materials and methods

2.1. Sample preparation and surface characterization

The Ni-free, Zr-based BMG plates were prepared by an injection-casting technique described elsewhere [14]. The microstructure of the BMG plates was analyzed using an X-ray diffractometer (XRD). The chemical composition (in at.%) of the BMG plates, analyzed using X-ray wavelength-dispersive spectroscopy (WDS), contained approximately 50 at.% Zr, 43 at.% Cu, and 7% Al. The BMG specimens were polished with a series of silicon carbide papers; #1200 was the finest grit used. This resulted in a surface roughness, R_a, of approximately 0.1 μm for the BMG specimens. Biomedical Ti plates, which are widely used and also have a surface roughness, R_a, of approximately 0.1 μm, were used as a comparison in the following tests of corrosion resistance and biocompatibility. The elastic modulus of polished BMG plates, measured using a Berkovich nanoindenter, was approximately 85 GPa, which was lower than that of polished Ti metal (approximately 100 GPa).

2.2. Corrosion resistance analysis

A potentiostat was used to perform the potentiodynamic polarization curve measurements. Acidic (pH 5.0) AS [15] and neutral (pH 7.4) SBF [16] were used as the corrosion test electrolytes. The test specimens were used as the working electrode, with an exposure area of approximately 1.76 cm^2. A platinum sheet and a saturated calomel electrode (SCE) were used as the counter electrode and the reference electrode, respectively. The potentiodynamic polarization curves of the test specimens were measured from −0.5 V (vs. SCE) in the anodic direction, with a scan rate of 1 mV/s. Measurement was stopped when the current density reached 1 mA/cm^2. The electrolyte was deaerated with nitrogen gas for 1 h before the corrosion test was started. The corrosion parameters, including corrosion potential (E_{corr}), corrosion rate (I_{corr}), pitting potential (E_{pit}), and $E_{pit} - E_{corr}$, were obtained from potentiodynamic polarization curves and used to evaluate the resistance of the test specimens to corrosion. At least five samples were used for each test condition.

2.3. Biocompatibility assay

2.3.1. Cytotoxicity

Two different mouse fibroblast cell lines (NIH 3T3 and L929) were used to assess the cytotoxicity of the extracts from the test specimens. The test specimens were extracted for 1 day in Dulbecco's modified Eagle's medium (DMEM) at 37 °C in a 5% CO$_2$ incubator. Then, the extracts were placed on cell monolayers for 1 day of incubation, after which the cells were examined for morphologic changes and cytolysis to determine a toxicity score.

The cell viability was investigated using an MTT (3-(4,5-dimethylthiazol-2-yl)-2,5-diphenyl tetrazolium bromide) assay. The cells were first washed with phosphate buffered saline (PBS), and then MTT (0.5 mg/ml) was added to the culture medium; next, the cells were incubated for 4 h at 37 °C. MTT was converted to a blue formazan dye by mitochondrial enzymes, and the dye was dissolved with isopropanol and measured with a microplate photometer at 570 nm. A higher optical density (OD) value represented higher cell viability. Additionally, the control groups for the cytotoxicity assay included a positive control (10% dimethyl sulfoxide (DMSO) in DMEM), a negative control (bioinert zirconia plate), and a reagent control (DMEM). More detailed experimental procedures are described in the ISO 10993-5 specification.

To quantify the ions released from the specimens, the specimens (exposure area: 1.76 cm^2) were immersed in cell culture medium (DMEM) at 37 °C in a 5% CO$_2$ incubator. After 1 day of immersion, the solution from each test group was collected for quantification of the ions released from the test specimens. The concentration of released metal ions (Zr, Cu, and Al ions for BMG specimens; Ti ions for Ti specimens) was measured using an inductively coupled plasma-atomic emission spectrometer (ICP-AES) and expressed in parts per billion (ppb).

2.3.2. Cell adhesion

hMSCs were seeded on the test specimens at a density of 5×10^4 cells/specimen. After 6 h of incubation, adherent cells were fixed with 2.5% glutaraldehyde for 2 h and then postfixed with 1% OsO$_4$ solution for 1 h at room temperature. Next, the test specimens were washed with deionized water and dehydrated in a sequential ethanol series (30%–100%) and with a critical point dryer. The test discs were coated with a thin platinum film, and the cell adhesion morphology was observed using a field emission-scanning electron microscope (FE-SEM). Meanwhile, the adherent cells from additional test specimens were fixed with 4% paraformaldehyde and permeabilized with 0.2% Triton X-100 in PBS. Then, cells were incubated with mouse monoclonal anti-vinculin at 4 °C overnight, secondary antibody was conjugated with fluorescein isothiocyanate. The F-actin and nuclei were then stained with rhodamine phalloidin and 4′,6-diamidino-2-phenylindole (DAPI), respectively. Cell images were taken using a multipurpose zoom microscope and analyzed with image analysis software (Image-Pro Express 6.0).

2.3.3. In situ cell migration

The hMSCs were transduced with the gene for green fluorescent protein (GFP) by retroviral delivery. A wound-healing assay was used to evaluate the migration of GFP-labeled hMSCs on the test specimens. Cells (5×10^4 cells/specimen) were seeded on the test specimens and cultured until confluency. Next, a pipette tip was used to create a straight scratch on the test specimens to simulate a surface wound approximately 250 μm in width. A fluorescence microscope was used to capture images during the in situ cell migration at 0, 2, and 4 h.

2.3.4. Protein adsorption

A bicinchoninic acid (BCA) assay was used to quantitatively evaluate protein adsorption. A solution containing 5 mg/mL albumin was spread over the whole surface of each test specimen. After different periods of incubation (30 and 60 min) at 37 °C, the adsorbed albumin was collected and mixed with BCA at 37 °C for 30 min. The albumin content was quantified using a Thermo Scientific Multiskan FC microplate photometer at 570 nm.

3. Results and discussion

3.1. Surface characterizations

Fig. 1 shows the XRD patterns of the as-cast $Zr_{50}Cu_{43}Al_7$ alloy, which contained only a broad peak near $2\theta = 38.6°$, indicating that the as-cast $Zr_{50}Cu_{43}Al_7$ alloy was basically amorphous.

Analysis of the XPS spectra (not shown) revealed that the oxide film on the outermost surface of the $Zr_{50}Cu_{43}Al_7$ contained (in atomic percent) 75.5% O, 19.8% Zr, 2.4% Cu, and 2.3% Al. This indicated that the surface oxide film was primarily composed of Zr oxide (as ZrO_2), with trace amounts of Cu and Al oxides. The presence of corrosion-resistant ZrO_2 on the outermost surface of $Zr_{50}Cu_{43}Al_7$ was expected to provide good corrosion resistance, which will be discussed later. Additionally, the absence of Ni in the $Zr_{50}Cu_{43}Al_7$ and the scant Cu on the outermost surface of the $Zr_{50}Cu_{43}Al_7$ could be expected to improve biocompatibility, as was verified by the following assays for cytotoxicity, cell adhesion, and cell migration.
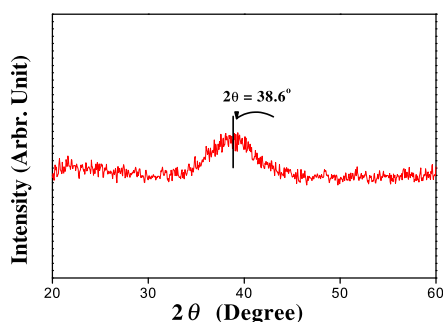
Fig. 1. XRD patterns of the cast $Zr_{50}Cu_{43}Al_7$ alloy, revealing only a broad peak near $2\theta = 38.6°$.

3.2. Corrosion resistance

Table 1 shows the corrosion parameters, obtained from the potentiodynamic polarization curve measurements, of $Zr_{50}Cu_{43}Al_7$ and Ti specimens in (a) SA and (b) SBF. $Zr_{50}Cu_{43}Al_7$ in AS and SBF showed a similar corrosion rate to that of Ti. This indicates that the corrosion rate of $Zr_{50}Cu_{43}Al_7$ specimens in SA and SBF was comparable to that of the widely used biomedical Ti. Additionally, the corrosion rates (0.21–0.23 $\mu A/cm^2$) of $Zr_{50}Cu_{43}Al_7$ in SA and PBF were much lower than those (0.39–2.13 $\mu A/cm^2$) of other Zr-based BMGs in simulated body environments [4]. Furthermore, pitting occurred only on $Zr_{50}Cu_{43}Al_7$ specimens. However, the potential at which pitting of $Zr_{50}Cu_{43}Al_7$ occurred in AS was 125 mV, which was much higher than the pitting potentials (near 0 mV) observed for other Ni-containing, Zr-based BMGs in simulated body environments [4,17].

The $E_{pit} - E_{corr}$ value is a sign of resistance to pit initiation, with larger values indicating higher resistance. In this study, the $E_{pit} - E_{corr}$ values were 535 and 388 mV in AS and SBF, respectively. These values were higher than that (380 mV) of ZrTiCuNiBe BMG in SBF [4] and those (265–355 mV) of ZrCuNiAlTi BMG in NaCl solution [18].

Previous research has shown that elemental Cu is prone to forming nanocrystals on the surface of Cu-containing, Zr-based BMGs. These Cu nanocrystals can accelerate the dissolution of BMGs by causing localized corrosion through the formation of a galvanic corrosion cell [19]. It is also believed that inhomogeneity within cast BMG alloys could result in localized imperfections in the surface passive film and lead to subsequent localized corrosion (e.g., pitting corrosion) [17]. The pitting resistance of the $Zr_{50}Cu_{43}Al_7$ BMG used in this study should be further improved by increasing the homogeneity and by decreasing the Cu content of the cast alloy when the pitting resistance is of a great concern in biomedical applications.

Table 1
Corrosion parameters, obtained from the potentiodynamic polarization curve measurements, of $Zr_{50}Cu_{43}Al_7$ BMG and Ti specimens in (a) artificial saliva (AS) and (b) simulated body fluid (SBF).

|	Corrosion rate (I_{corr}, $\mu A/cm^2$)	Pitting potential (E_{pit}, mV)	Corrosion potential (E_{corr}, mV)	$E_{pit} - E_{corr}$ (mV)
(a) In AS				
Ti	0.19	NA	−495	NA
BMG	0.23	125	−410	535
(b) In SBF				
Ti	0.11	NA	−583	NA
BMG	0.21	−162	−550	388

NA: not available.

3.3. Biocompatibility

Fig. 2 shows the viability of (a) NIH 3T3 and (b) L929 cells cocultured with extracts from the $Zr_{50}Cu_{43}Al_7$ BMG and Ti specimens. Both NIH 3T3 and L929 cells cultured in the extract-containing media (BMG and Ti) had a similar or even slightly higher cell viability compared with cells cultured in the reagent control and the negative control. The $Zr_{50}Cu_{43}Al_7$ BMG and Ti groups had very similar cell viabilities, indicating that the $Zr_{50}Cu_{43}Al_7$ BMG alloy was not cytotoxic and that its biocompatibility, in terms of cell viability, was comparable to that of the widely used biomedical Ti metal.

Table 2 shows the ion release from $Zr_{50}Cu_{43}Al_7$ BMG and Ti specimens after 1 day of immersion in cell culture medium (DMEM). Ti and Zr are believed to be favorable nontoxic metals with good biocompatibility [20,21]. Note that the total ion release from the $Zr_{50}Cu_{43}Al_7$ specimen after 1 day of immersion in cell culture medium was below 100 ppb, which was close to that from the Ti specimen.

Cu ion is a necessary nutrient; however, excessive Cu ions may lead to biological toxicity [22]. Generally, most diets contain enough Cu (2–5 mg) for a daily intake but not enough to cause toxicity. The World Health Organization (WHO) suggests that 10–12 mg per day may possibly be the upper safe concentration for consumption. In this study, the concentration of Cu ion released from the BMG specimen after 1 day of immersion in DMEM was below 50 ppb, which is much lower than that contained in most diets and well below the safe level suggested by the WHO. It is well known that Al is related to neurotoxicity and senile dementia of the Alzheimer type [23,24]. Al ion can exhibit cytotoxicity when its concentration
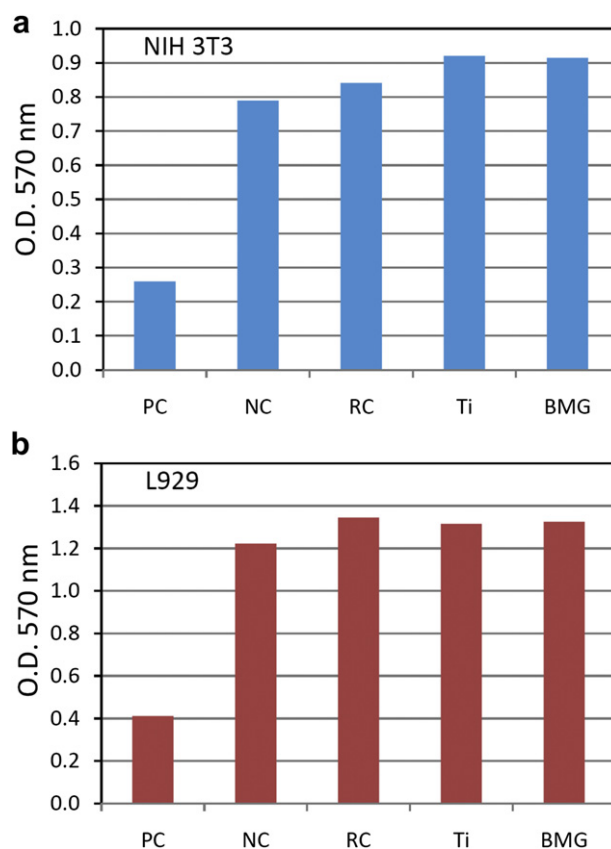

Fig. 2. ISO 10993-5 cytotoxicity assay results, showing the viability of NIH 3T3 and L929 cells cultured in the extract-containing media. PC: positive control; NC: negative control; RC: reagent control; Ti: Ti specimen; BMG: $Zr_{50}Cu_{43}Al_7$ specimen.

Table 2
Ion release (ppb) from $Zr_{50}Cu_{43}Al_7$ BMG and Ti specimens after 1 day of immersion in cell culture medium (DMEM).

	BMG			Ti
Ion	Zr	Cu	Al	Ti
Concentration (ppb)	54	33	4	97

is higher than 200 ppb [25]. In this study, the concentration of Al ion released from the BMG specimen after 1 day of immersion in culture medium was 4 ppb, which is 50 times lower than the level that causes cytotoxicity. It was clear that the nontoxicity of $Zr_{50}Cu_{43}Al_7$ was mainly due to the very low corrosion rate and, in particular, the very low level of ion release, ascribed to the presence of a protective ZrO_2 surface film on the $Zr_{50}Cu_{43}Al_7$ specimens.
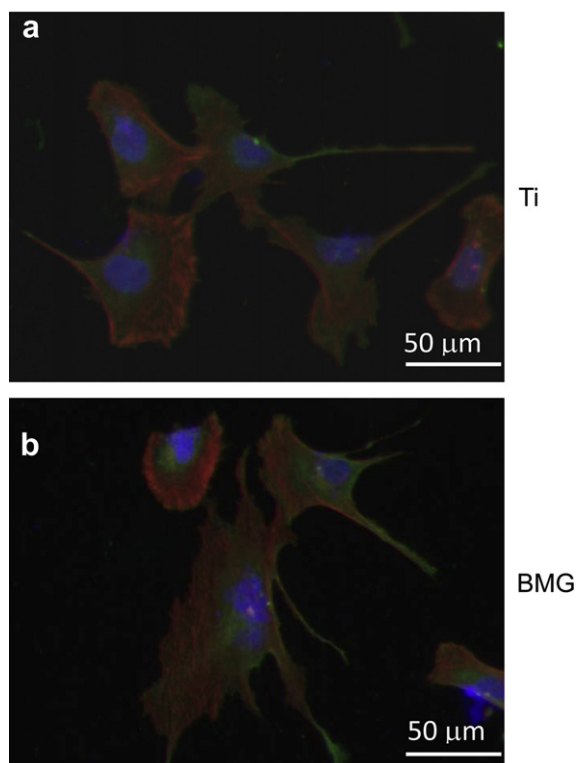
The morphology of hMSCs growing on Ti and $Zr_{50}Cu_{43}Al_7$ surfaces was investigated using both immunofluorescent staining (Fig. 3) and FE-SEM observations (Fig. 4). After 6 h of incubation, the attached hMSCs were observed spreading on the $Zr_{50}Cu_{43}Al_7$ BMG surface (Fig. 3(b)) with organized F-actin stress fibers (red). The presence of filopodia, which are important in cell migration, was confirmed by the focal adhesions formed between the cell and the substrate through vinculin proteins (green). This observation suggests that the $Zr_{50}Cu_{43}Al_7$ BMG surface supported initial hMSC attachment and spreading, which are necessary for further cellular functions such as proliferation and differentiation. Fig. 4 shows FE-SEM images of hBMCs on Ti and $Zr_{50}Cu_{43}Al_7$ BMG surfaces after 6 h of cell incubation. A flattened cell morphology with extended filopodia was observed on the $Zr_{50}Cu_{43}Al_7$ BMG surface (Fig. 4 (b)). This confirmed the immunofluorescence results (Fig. 3(b)) indicating that the hMSCs used filopodia to form focal adhesions with the material surface and to connect with adjacent cells. Note that cells attached to the
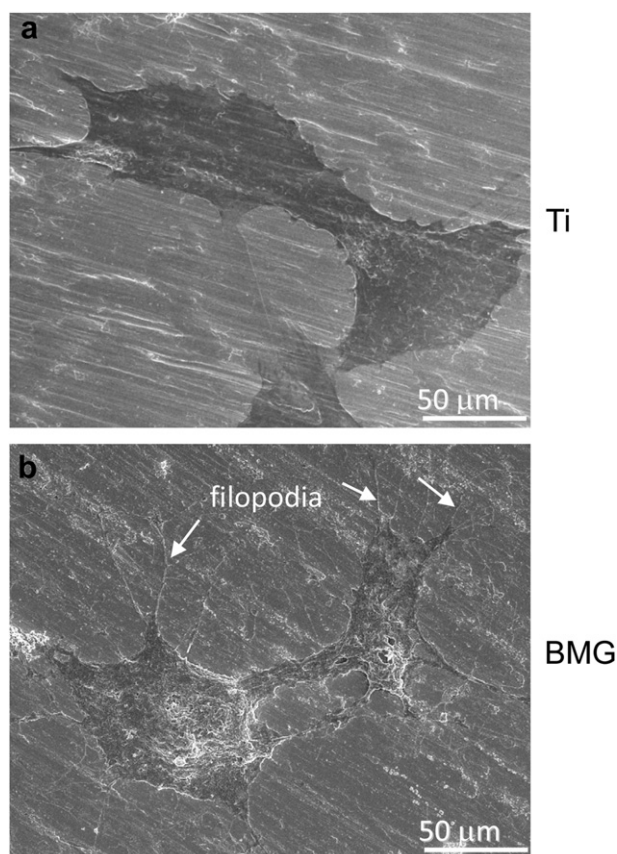

Fig. 4. FE-SEM observations of adhesion morphology of hMSCs on Ti and $Zr_{50}Cu_{43}Al_7$ BMG surfaces after 6 h of incubation, showing flattened cell morphology with extended filopodia on BMG surface.

$Zr_{50}Cu_{43}Al_7$ BMG surface had more extended filopodia than did cells attached to the Ti surface, indicating that the $Zr_{50}Cu_{43}Al_7$ BMG used in this study had a better cell adhesion morphology.

Fig. 5 shows the *in situ* directional cell migration on Ti and $Zr_{50}Cu_{43}Al_7$ BMG surfaces using a wound-healing assay over 4 h. More cells migrated toward the wound on the $Zr_{50}Cu_{43}Al_7$ BMG surface than on the Ti surface, and the wound on the BMG surface was nearly covered by cells after 4 h of incubation. The estimated

Fig. 3. Immunofluorescent staining analysis of hMSCs growing on Ti and $Zr_{50}Cu_{43}Al_7$ BMG surfaces after 6 h of incubation, showing focal adhesion (green) and F-actin stress fibers (red) on both surfaces. (For interpretation of the references to color in this figure legend, the reader is referred to the web version of this article.)
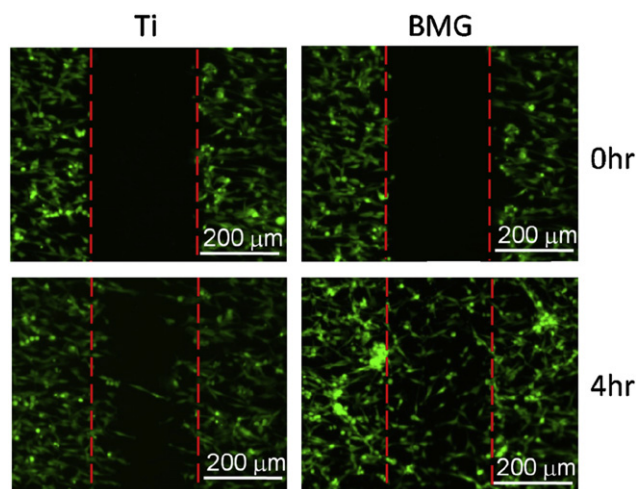
Fig. 5. Wound-healing assay results, showing the *in situ* directional cell migration on Ti and $Zr_{50}Cu_{43}Al_7$ BMG surfaces at time points of 0 and 4 h.
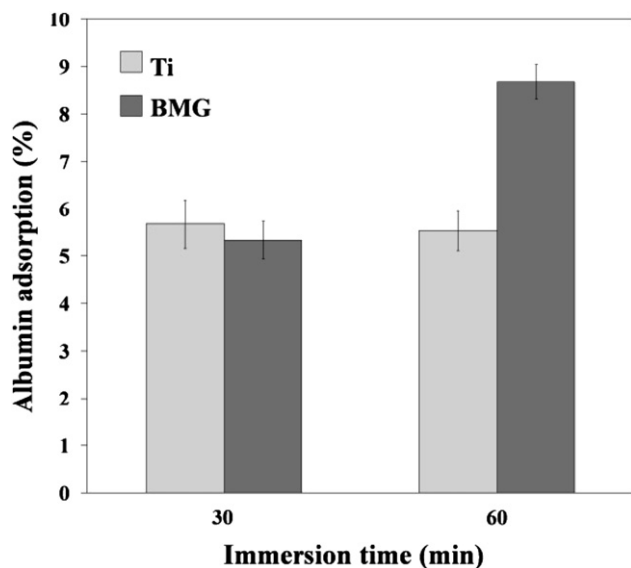
Fig. 6. BCA assay results, showing the albumin adsorption on Ti and $Zr_{50}Cu_{43}Al_7$ BMG after 30- and 60-min immersion in albumin-containing solution (error bar: standard deviation).

cell migration rates on the BMG and Ti surfaces were approximately 30 μm/h and 16 μm/h, respectively. This implies that the $Zr_{50}Cu_{43}Al_7$ BMG surface supported cell migration better than the Ti surface. Further investigations on cell proliferation and differentiation are now in progress in order to evaluate the potential of $Zr_{50}Cu_{43}Al_7$ BMG for long-term clinical applications.

Albumin adsorption on Ti and $Zr_{50}Cu_{43}Al_7$ BMG after 30- and 60-min immersion in albumin-containing solution was analyzed using a BCA assay, and the results are shown in Fig. 6. Compared with the Ti surface, the $Zr_{50}Cu_{43}Al_7$ BMG surface had similar albumin adsorption after 30 min of immersion in the albumin-containing solution. However, after 60 min of contact with albumin, the $Zr_{50}Cu_{43}Al_7$ BMG surface had approximately 1.6 times more albumin adsorption than the Ti surface. More adsorbed proteins on biomaterials can provide more sites for cells to bond to the material surface, which may increase cell adhesion and then enhance subsequent bone growth and implant stabilization [26,27]. This could partially explain the fact that better cell adhesion morphology (Figs. 3 and 4) and faster cell migration (Fig. 5) were observed on the $Zr_{50}Cu_{43}Al_7$ surface than on the Ti surface. However, the reason why the $Zr_{50}Cu_{43}Al_7$ BMG surface had greater protein adsorption than the pure Ti surface needs further investigation.

4. Conclusions

Compared with widely used biomedical Ti, nontoxic $Zr_{50}Cu_{43}Al_7$ BMG had a comparable corrosion rate, better cell adhesion morphology, and higher levels of cell migration and protein adsorption. This suggests that $Zr_{50}Cu_{43}Al_7$ BMG has the potential to be used for biomedical applications. However, further improvements to the pitting corrosion resistance of $Zr_{50}Cu_{43}Al_7$ BMG in biological environments should be made before proceeding to *in vivo* animal studies.

References

[1] Hiromoto S, Hanawa T. Re-passivation current of amorphous $Zr_{65}Al_{7.5}Ni_{10}Cu_{17.5}$ alloy in a Hanks' balanced solution. Electrochim Acta 2002;47: 1343–9.
[2] Jin K, Löffler JF. Bulk metallic glass formation in Zr–Cu–Fe–Al alloys. Appl Phys Lett 2005;86. p. 241909-1–241909-3.
[3] Huang L, Qiao D, Green BA, Liaw PK, Wang J, Pang S, et al. Bio-corrosion study on zirconium-based bulk-metallic glasses. Intermetallics 2009;17: 195–9.
[4] Wang YB, Li HF, Zheng YF, Wei SC, Li M. Correlation between corrosion performance and surface wettability in ZrTiCuNiBe bulk metallic glasses. Appl Phys Lett 2010;96. p. 251909-1–251909-3.
[5] He W, Chuang A, Cao Z, Liaw PK. Biocompatibility study of zirconium-based bulk metallic glasses for orthopedic applications. Metall Mater Trans 2010; 41A:1726–34.
[6] International Agency for Research on Cancer (IARC) monographs on the evaluation of carcinogenic risks to humansSurgical implants and other foreign bodies, vol. 74. Lyon: IARC Press; 1999.
[7] Wataha JC, Lockwood PE, Schedle A. Effect of silver, copper, mercury, and nickel ions on cellular proliferation during extended, low-dose exposures. J Biomed Mater Res 2000;52:360–4.
[8] Qiu CL, Chen Q, Liu L, Chan KC, Zhou JX, Chen PP, et al. A novel Ni-free Zr-based bulk metallic glass with enhanced plasticity and good biocompatibility. Scripta Mater 2006;55:605–8.
[9] Liu L, Qiu CL, Chen Q, Chan KC, Zhang SM. Deformation behavior, corrosion resistance, and cytotoxicity of Ni-free Zr-based bulk metallic glasses. J Biomed Mater Res 2008;86A:160–9.
[10] Liu L, Qiu CL, Huang CY, Yu Y, Huang H, Zhang SM. Biocompatibility of Ni-free Zr-based bulk metallic glasses. Intermetallics 2009;17:235–40.
[11] Morrison ML, Buchanan RA, Leon RV, Liu CT, Green BA, Liaw PK, et al. The electrochemical evaluation of a Zr-based bulk metallic glass in a phosphate-buffered saline electrolyte. J Biomed Mater Res 2005;74A:430–8.
[12] Kanayama M, Cunningham BW, Haggerty CJ, Abumi K, Kaneda K, McAfee PC. In vitro biomechanical investigation of the stability and stress-shielding effect of lumbar interbody fusion devices. J Neurosurg 2000;93:259–65.
[13] Fu QG, Liu XW, Xu SG, Li M, Zhang CC. Stress-shielding effect of nitinol swan-like memory compressive connector on fracture healing of upper limb. J Mater Eng Perform 2009;18:797–804.
[14] Löser W, Das J, Güth A, Klauß HJ, Mickel C, Kühn U, et al. Effect of casting conditions on dendrite-amorphous/nanocrystalline Zr–Nb–Cu–Ni–Al in situ composites. Intermetallics 2004;12:1153–8.
[15] Huang HH. Effect of fluoride and albumin concentration on the corrosion behavior of Ti-6Al-4V alloy. Biomaterials 2003;24:275–82.
[16] Yang CH, Wang YT, Tsai WF, Ai CF, Lin MC, Huang HH. Effect of oxygen plasma immersion ion implantation treatment on corrosion resistance and cell adhesion of titanium surface. Clin Oral Implants Res 2011;22:1426–32.
[17] Morrison ML, Buchanan RA, Peker A, Peter WH, Horton JA, Liaw PK. Cyclic-anodic-polarization studies of a $Zr_{41.2}Ti_{13.8}Ni_{10}Cu_{12.5}Be_{22.5}$ bulk metallic glass. Intermetallics 2004;12:1177–81.
[18] Jiang WH, Jiang F, Green BA, Liu FX, Liaw PK, Choo H, et al. Electrochemical corrosion behavior of a Zr-based bulk-metallic glass. Appl Phys Lett 2007;91. p. 041904-1–041904-3.
[19] Paillier J, Mickel C, Gostin PF, Gebert A. Characterization of corrosion phenomena of Zr–Ti–Cu–Al–Ni metallic glass by SEM and TEM. Mater Charact 2010;61:1000–8.
[20] Wang X, Li Y, Hodgson PD, Wen C. Biomimetic modification of porous TiNbZr alloy scaffold for bone tissue engineering. Tissue Eng Part A 2010;16: 309–16.
[21] Steinemann SG. Corrosion of surgical implants — in vivo and in vitro tests. In: Winter GD, Leray JL, de Goot K, editors. Evaluation of biomaterials. New York: John Wiley and Sons Inc.; 1980. p. 1–34.
[22] Lee JA, Marsden ID, Glover CN. The influence of salinity on copper accumulation and its toxic effects in estuarine animals with differing osmoregulatory strategies. Aquat Toxicol 2010;99:65–72.
[23] Landsberg JP, McDonald B, Watt F. Absence of aluminium in neurotic plaque cores in Alzheimer's disease. Nature 1992;360:65–8.
[24] Farrar G, Altmann P, Welch S, Wychrij O, Ghose B, Lejeune J, et al. Defective gallium-transferrin binding in Alzheimer disease and Down syndrome: possible mechanism for accumulation of aluminium in brain. Lancet 1990; 335:747–50.
[25] Okazaki Y, Rao S, Ito Y, Tateishi T. Corrosion resistance, mechanical properties, corrosion fatigue strength and cytocompatibility of new Ti alloys without Al and V. Biomaterials 1998;19:1197–215.
[26] Degasne I, Baslé MF, Demais V, Huré G, Lesourd M, Grolleau B, et al. Effects of roughness, fibronectin and vitronectin on attachment, spreading, and proliferation of human osteoblast-like cells (Saos-2) on titanium surfaces. Calcif Tissue Int 1999;64:499–507.
[27] Deligianni DD, Katsala N, Ladas S, Sotiropoulou D, Amedee J, Missirlis YF. Effect of surface roughness of the titanium alloy Ti-6Al-4V on human bone marrow cell response and on protein adsorption. Biomaterials 2001;22: 1241–51.